Spin correlation coefficient for proton-^{3}He elastic scattering at 100 MeV

A. Watanabe,[1,*] S. Nakai,[2,3] K. Sekiguchi,[1,2,†] A. Deltuva,[4] S. Goto,[5] K. Hatanaka,[6] Y. Hirai,[5] T. Ino,[7] D. Inomoto,[5] M. Inoue,[2] S. Ishikawa,[8] M. Itoh,[9] H. Kanda,[6] H. Kasahara,[5] Y. Maeda,[10] K. Miki,[2] K. Nonaka,[10] H. J. Ong,[6,11] H. Oshiro,[5] D. Sakai,[2] H. Sakai,[12] S. Shibuya,[2] D. T. Tran,[13] H. Umetsu,[2] Y. Utsuki,[2] and T. Wakasa[5]

[1]*Department of Physics, Tokyo Institute of Technology, Tokyo 152-8551, Japan*
[2]*Department of Physics, Tohoku University, Sendai 980-8578, Japan*
[3]*Graduate Program on Physics for the Universe (GP-PU), Tohoku University, Sendai 980-8578, Japan*
[4]*Institute of Theoretical Physics and Astronomy, Vilnius University, Saulėtekio al. 3, LT-10257 Vilnius, Lithuania*
[5]*Department of Physics, Kyushu University, Fukuoka 819-0395, Japan*
[6]*Research Center for Nuclear Physics, Osaka University, Ibaraki 567-0047, Japan*
[7]*High Energy Accelerator Research Organization (KEK), Tsukuba 305-0801, Japan*
[8]*Science Research Center, Hosei University, Tokyo 102-8160, Japan*
[9]*Cyclotron and Radioisotope Center, Tohoku University, Sendai 980-8578, Japan*
[10]*Faculty of Engineering, University of Miyazaki, Miyazaki 889-2192, Japan*
[11]*Institute of Modern Physics (IMP), Chinese Academy of Sciences, Lanzhou 730000, China*
[12]*RIKEN Nishina Center, Wako 351-0198, Japan*
[13]*Institute of Physics, Vietnam Academy of Science and Technology, Hanoi 10000, Vietnam*

(Received 29 July 2022; accepted 17 October 2022; published 21 November 2022)

We present the measured spin correlation coefficient $C_{y,y}$ for p-^{3}He elastic scattering at 100 MeV at the angles $\theta_{\mathrm{c.m.}} = 46.9°$–$149.2°$ in the center-of-mass system. The $C_{y,y}$ data and the existing cross section data are compared with rigorous four-nucleon scattering calculations based on realistic nucleon-nucleon potentials. Large differences are seen in the regime around the cross section minimum for both observables. The Δ-isobar effects estimated by the $NN + N\Delta$ coupled-channels approach are small for the cross section. Meanwhile, in $C_{y,y}$, the Δ-isobar effects improve the agreement with the data. The analysis of the p-^{3}He elastic scattering amplitudes implies the necessity of three-nucleon forces (3NFs) that enhance the vector components in the amplitudes. The obtained results indicate that the spin correlation coefficient $C_{y,y}$ expands the knowledge of the nuclear interactions with the Δ isobar or those including 3NFs that are masked in nucleon-deuteron elastic scattering.

DOI: 10.1103/PhysRevC.106.054002

I. INTRODUCTION

One of the open questions in nuclear physics nowadays is a complete knowledge of the interactions among nucleons. Modern realistic nucleon-nucleon (NN) potentials like AV18 [1], CD Bonn [2], Nijmegen I and II [3], or those based on chiral effective field theory (χEFT) [4], which reproduce the NN observables up to 350 MeV with very high precision, do not describe well various nuclear phenomena [5,6]. Three-nucleon forces (3NFs), which appear when more than two nucleons interact, have been suggested as possible candidates to improve the situation. Few-nucleon scattering systems, where numerically exact solutions for any two-nucleon (2N) and 3N forces are feasible, play especially important roles in the investigations of the nuclear interactions. In 3N scattering, extensive experimental and theoretical studies of the nucleon-deuteron (N-d) scattering have been performed in a wide range of incoming nucleon energies up to $E \approx 300$ MeV/nucleon. Sizable discrepancies between the data and rigorous numerical calculations with realistic NN potentials in the cross section minimum region were successfully explained by inclusion of the two-pion exchange 3NF models [7–9], or substantially reduced by calculations in an extended Hilbert space which allow the explicit excitation of a nucleon to a Δ isobar, yielding an effective 3NF [10,11]. In the approach from the χEFT, it has been reported that the deuteron-proton (d-p) elastic cross section at 70 MeV/nucleon [12] constrains low-energy constants of 3NFs [13]. Together with this, the necessity of the fourth- and fifth-order of the χEFT 3NFs is indicated for the description of the spin observables in the N-d scattering at intermediate energies [14].

Study of nuclear interactions has recently been extended to the four-nucleon (4N) scattering at intermediate energy in the p-^{3}He system [15]. High precision data for the cross section $d\sigma/d\Omega$, proton and ^{3}He analyzing powers, and spin correlation coefficient $C_{y,y}$ at the incident proton energy near 65 MeV are compared with rigorous numerical calculations of 4N-scattering based on various NN potentials without the Coulomb force. Clear discrepancies have been found for some of the measured observables, especially in the angular regime

*atomu@phys.titech.ac.jp
†kimiko@phys.titech.ac.jp

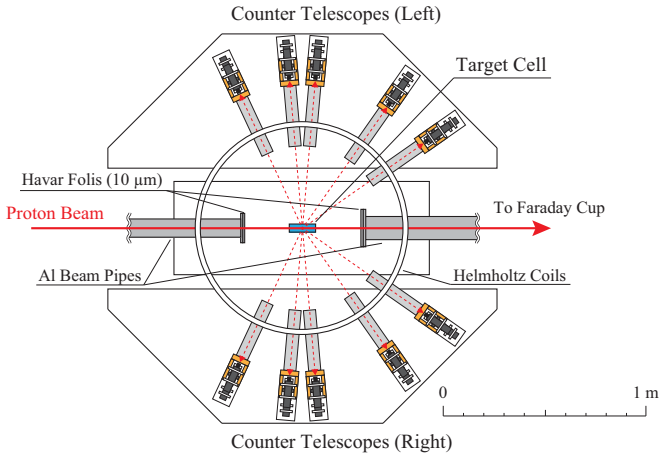

FIG. 1. Schematic layout of the experimental setup for the measurement of the spin correlation coefficient.

around the $d\sigma/d\Omega$ minimum. The Δ-isobar effects, estimated by the $NN + N\Delta$ coupled-channels approach, do not remedy the differences, in contrast to the N-d elastic scattering in the same energy regime [10,11]. A small total Δ-isobar effect in the $d\sigma/d\Omega$ is because of cancellation between the effects of $2N$ dispersion and those of the effective $3N$ and $4N$ forces. Meanwhile, a total Δ-isobar effect is predicted to be large in the spin correlation coefficient $C_{y,y}$ for which the cancellation has not occurred. However, the measured data at limited angles are insufficient for firm conclusions regarding the Δ-isobar effects in $C_{y,y}$.

The results of Ref. [15] present a new challenge to be solved, showing that p-^{3}He elastic scattering at intermediate energies is an excellent tool to explore the nuclear interactions that could not be accessible in N-d scattering. In this paper, we present the measured spin correlation coefficient $C_{y,y}$ at 100 MeV at the angles $\theta_{\rm c.m.} = 46.9°$–$149.2°$ in the center-of-mass system (c.m.). The data are compared with rigorous numerical calculations for $4N$-scattering based on realistic NN potentials as well as with the Δ-isobar excitation. Together with this, by using the newly obtained $C_{y,y}$ data and the existing cross section data [16], we discuss how these two observables are related to the elastic scattering amplitudes in view of investigating the difference between the p-^{3}He and d-p scattering systems.

Our paper is organized as follows. In Sec. II, we describe the experimental procedure and the data analysis. Discussion follows in Sec. III. Finally, we summarize and conclude in Sec. IV.

II. EXPERIMENTAL PROCEDURE AND DATA ANALYSIS

The measurement of the spin correlation coefficient $C_{y,y}$ was performed using a 100 MeV polarized proton beam in conjunction with the polarized ^{3}He target [17] in the East Experimental Hall at the Research Center for Nuclear Physics (RCNP), Osaka University. A schematic layout of the experimental setup around the target is shown in Fig. 1. A polarized proton beam provided by an atomic beam polarized ion source [18] was accelerated up to 21.9 MeV by the AVF cyclotron, and then up to 100 MeV by the Ring cyclotron. The beam was transported to the polarized ^{3}He target at the ENN beam line and it was stopped in a Faraday cup. Typical beam intensity was 30 nA. The beam polarization was measured continuously with a beamline polarimeter prior to acceleration by the Ring cyclotron using p-^{12}C elastic scattering at 21.9 MeV [19]. In the present measurement typical value of the beam polarization was 0.45.

The same polarized ^{3}He target system as in Ref. [15] was applied to the measurement of $C_{y,y}$ at 100 MeV. The vacuum was separated by Havar foils with thickness of 10 μm, allowing operation of the target and the detector system in atmosphere. To detect scattered protons from the ^{3}He target, sets of counter telescopes were positioned 730 mm away from the center of the target cell on each side symmetrical to the beam axis. The measured angles were $\theta_{\rm lab.} = 35.0°$–$135.0°$ in the laboratory system which corresponds to $\theta_{\rm c.m.} = 46.9°$–$149.2°$ in the center-of-mass system. Each counter telescope consisted of a NaI(Tl) scintillator and a plastic scintillator. The dimension of the NaI(Tl) scintillator was 50 mm (thickness) $\times$31 mm (width) $\times$ 31 mm (height). For the plastic scintillators, different thickness, namely 0.5, 1.0, and 2.0 mm, was applied depending on the measured angles. A double-slit collimator, which was made of 25-mm-thick brass both for the front and rear parts, was used to define the target volume and the solid angle for each counter telescope.

A spin-exchange optical pumping (SEOP) ^{3}He target [20,21] was used to perform the spin-correlation coefficient measurement. A double-chambered cell, in which target and pumping chambers were connected by a thin transfer tube, made of GE180 glass was used for the measurement. The target cell was filled with 3 atm of ^{3}He gas at room temperature, a small amount of N_2 gas (0.1 atm), and a mixture of Rb and K alkali metals. The pumping chamber was heated to about 500 K to provide sufficient high alkali-metal vapor density. Circularly polarized laser light at 794.7 nm with power of 60 W was used to polarize Rb atoms in the pumping chamber. The polarization of alkali metals was transferred to ^{3}He nuclei through spin exchange interactions in the pumping chamber and then the polarized ^{3}He gas diffused into the target chamber. A pair of Helmholtz coils with 100 cm diameter provided a 12 G magnetic field to define the direction of the ^{3}He nuclear polarization which was aligned to the vertical axis. The target chamber of the target cell was 4 cm in diameter and 15 cm long along the beam path. The entrance and exit windows had a thin thickness of 0.4 mm, and the side surfaces, where scattered protons passed, had a thickness of about 1 mm. During the measurement the ^{3}He polarization was monitored by the adiabatic fast passage NMR method. The direction of the polarization was reversed every hour. The ^{3}He polarization was measured using the electron paramagnetic resonance (EPR) technique [22]. The absolute values of the target polarization were determined by the thermal neutron transmission using RIKEN Accelerator-driven compact Neutron Source (RANS) [23], and were consistent with the results of the EPR measurements. The NMR signal was calibrated based on the results of the neutron transmission measurement. The typical target polarization was 0.34 during the measurement.

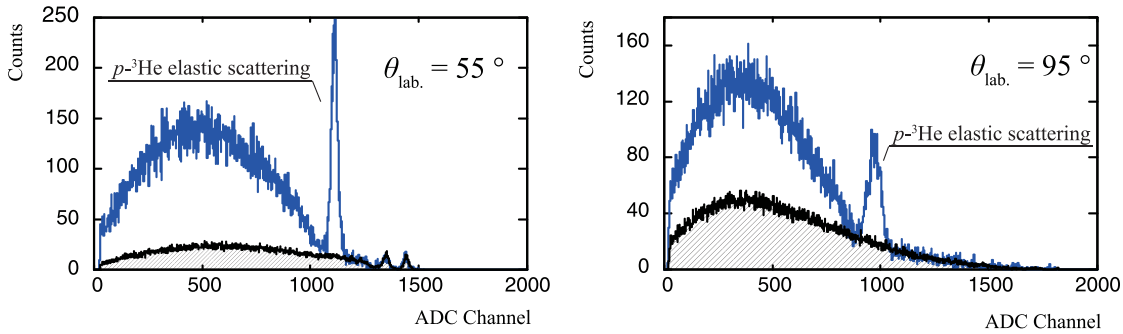

FIG. 2. Light output spectra of scattered protons obtained by the NaI(Tl) scintillators at $\theta_{\text{lab.}} = 55°$ and 95°. The hatched regions indicate events obtained with the reference cell.

A more detailed description of the target system is found in Refs. [17,24,25].

Figure 2 shows the light output spectra for the scattered protons obtained by NaI(Tl) scintillators at the laboratory angles of $\theta_{\text{lab.}} = 55°$ and 95° ($\theta_{\text{c.m.}} = 71.9°$ and 115.5°). The narrow peaks correspond to protons elastically scattered from ^{3}He. The events seen below the p-^{3}He elastic peaks are from the inelastic p-^{3}He scattering. A reference cell which is mostly identical to the target chamber of the ^{3}He cell and filled with 0.1 atm of N_2 gas was employed for estimating the background events. The background events from the alkali metals are assumed to be negligibly small due to the small number of their vapor densities. As shown in the figure, the backgrounds have an almost linear structure around the peak of elastic p-^{3}He scattering. The reference cell had slightly different glass thicknesses and the amount of N_2 gas from those of the ^{3}He cell. Thus the net yields of elastic p-^{3}He scattering were extracted by subtracting the background yields, whose function was assumed to be a linear one. The inelastic scattering events, which are well separated from the elastic scattering ones, contribute sufficiently small to the background subtraction.

The spin-dependent p-^{3}He scattering cross section $(d\sigma/d\Omega)$ for both the beam and ^{3}He target polarized, is given as follows:

$$\left(\frac{d\sigma}{d\Omega}\right) = \left(\frac{d\sigma}{d\Omega}\right)_0 \left(1 + p_y A_y + p_y^T A_{0y} + p_y p_y^T C_{y,y}\right). \quad (1)$$

Here $(d\sigma/d\Omega)_0$ denotes the unpolarized cross sections, while p_y and p_y^T are the polarizations of the proton beam and the ^{3}He target, respectively. In the measurement, both the beam and the target polarizations were aligned to the vertical direction. The measured yields of the possible combinations of the beam and the target by the detectors placed in the left (L) and right (R) sides are expressed as

$$\begin{aligned}
Y^L_{\uparrow\uparrow} &= \left(\frac{d\sigma}{d\Omega}\right)_0 \left(1 + p_y A_y + p_y^T A_y^T + p_y p_y^T C_{y,y}\right),\\
Y^L_{\uparrow\downarrow} &= \left(\frac{d\sigma}{d\Omega}\right)_0 \left(1 + p_y A_y - p_y^T A_y^T - p_y p_y^T C_{y,y}\right),\\
Y^L_{\downarrow\uparrow} &= \left(\frac{d\sigma}{d\Omega}\right)_0 \left(1 - p_y A_y + p_y^T A_y^T - p_y p_y^T C_{y,y}\right),\\
Y^L_{\downarrow\downarrow} &= \left(\frac{d\sigma}{d\Omega}\right)_0 \left(1 - p_y A_y - p_y^T A_y^T + p_y p_y^T C_{y,y}\right),\\
Y^R_{\uparrow\uparrow} &= \left(\frac{d\sigma}{d\Omega}\right)_0 \left(1 - p_y A_y - p_y^T A_y^T + p_y p_y^T C_{y,y}\right),\\
Y^R_{\uparrow\downarrow} &= \left(\frac{d\sigma}{d\Omega}\right)_0 \left(1 - p_y A_y + p_y^T A_y^T - p_y p_y^T C_{y,y}\right),\\
Y^R_{\downarrow\uparrow} &= \left(\frac{d\sigma}{d\Omega}\right)_0 \left(1 + p_y A_y - p_y^T A_y^T - p_y p_y^T C_{y,y}\right),\\
Y^R_{\downarrow\downarrow} &= \left(\frac{d\sigma}{d\Omega}\right)_0 \left(1 + p_y A_y + p_y^T A_y^T + p_y p_y^T C_{y,y}\right), \quad (2)
\end{aligned}$$

where Y is the measured yield normalized to the number of the incident beams, the target thickness and the solid angle of the detector. The first and second arrows (up or down) in the subscripts indicate the spin direction of the beam and the target, respectively. Then, the spin correlation coefficient $C_{y,y}$ is given by the relation

$$C_{y,y} = \frac{1}{p_y\, p_y^T} \frac{X-1}{X+1}, \quad (3)$$

where

$$X = \sqrt{\frac{Y^L_{\uparrow\uparrow} + Y^L_{\downarrow\downarrow}}{Y^L_{\uparrow\downarrow} + Y^L_{\downarrow\uparrow}}} \sqrt{\frac{Y^R_{\uparrow\uparrow} + Y^R_{\downarrow\downarrow}}{Y^R_{\uparrow\downarrow} + Y^R_{\downarrow\uparrow}}}. \quad (4)$$

To obtain $C_{y,y}$ values, the beam charge collected by the Faraday cup was used as the number of incident beams. For the beam (target) polarization p_y (p_y^T), the average value between the spin-up and spin-down modes was applied. The differences between the two spin modes were less than 3%, and were taken as systematic uncertainties.

Figure 3 shows the experimental results for the spin correlation coefficient $C_{y,y}$ with solid circles. The statistical error of the $C_{y,y}$ varies between 0.01 and 0.06 depending on the measured angles. The systematic error that came from the uncertainty of the target and beam polarization is estimated to be 0.01 or less. The systematic error due to false asymmetry estimated by the measurement where both the beam and target were unpolarized does not exceed the statistical uncertainty except for the most forward angle.

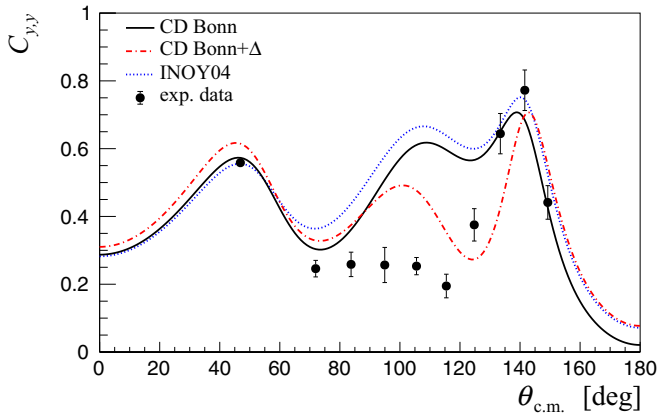

FIG. 3. Angular distributions of the spin correlation coefficient $C_{y,y}$ for p-^{3}He elastic scattering at 100 MeV. Experimental data (solid circles) are compared with the calculations from the solutions of exact AGS equations. Only statistical errors are indicated. Calculations based on the NN potentials are shown with black solid (CD Bonn) and blue dotted (INOY04) lines. The red dot-dashed line is the calculation based on the CD Bonn+Δ potential.

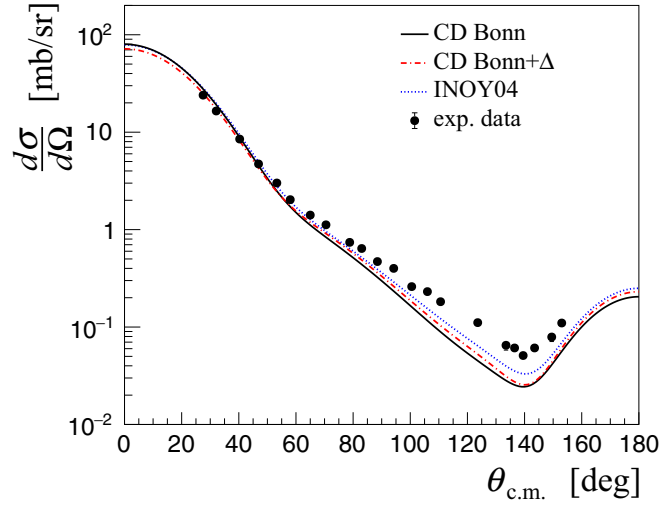

FIG. 4. Angular distributions of the cross section $d\sigma/d\Omega$ for p-^{3}He elastic scattering at 100 MeV. Data are from Ref. [16]. For descriptions of the calculations, see Fig. 3.

III. DISCUSSION

A. Comparison of data with theoretical calculations

The measured spin correlation coefficient $C_{y,y}$ is shown in Fig. 3 as a function of the c.m. scattering angle $\theta_{\text{c.m.}}$ and compared with the theoretical calculations. The observables for the p-^{3}He elastic scattering were calculated from the solutions of exact Alt-Grassberger-Sandhas (AGS) equations as given in Refs. [26,27] using the NN potentials CD Bonn [2] and INOY04 [28]. The calculations based on the CD Bonn+Δ model [11], which allows an excitation of a nucleon to a Δ isobar and thereby yields effective 3NFs and 4NFs, are also presented. The AGS equations for 4N transition operators are solved in the momentum-space partial wave representation [26] including NN waves with total angular momentum below 4. Since the rigorous treatment of the Coulomb force requires the inclusion of much higher partial waves, the Coulomb force is omitted in the present study. Given relatively high energy, it is expected to be significant at small angles up to $\theta_{\text{c.m.}} \approx 40^\circ$ only. The $C_{y,y}$ data at the angles $\theta_{\text{c.m.}} = 80^\circ$–$130^\circ$ deviate from the calculations with the NN potentials. The CD Bonn+Δ calculation provides sizable Δ-isobar effects at $\theta_{\text{c.m.}} = 100^\circ$–$140^\circ$. The predicted Δ-isobar effects improve the agreement with the data, but differences still remain in the angular regime around $\theta_{\text{c.m.}} = 100^\circ$.

In Fig. 4, the cross section $d\sigma/d\Omega$ data reported in Ref. [16] are shown in comparison with the calculations. The calculations with the NN potentials underestimate the data at the angles $\theta_{\text{c.m.}} \gtrsim 60^\circ$. The INOY04, which is fitted to reproduce ^{3}He binding energy, provides a better description of the data, but it still underestimates the experimental data. Δ-isobar effects are small, and are estimated by the difference between the CD Bonn+Δ and CD Bonn calculations. These features are similar to those observed at 65 MeV, leading to the conclusion of the necessity to incorporate additional 3NFs for the description of $d\sigma/d\Omega$ [15].

To study the Δ-isobar effects in more detail, the effects of the 2N dispersion, [Δ(disp.)], and those of 3N- and 4N-forces, [$\Delta(3N+4N)$], are singled out separately as in Refs. [15,26]. The results for the cross section are shown in Fig. 5(a) as a ratio to the calculation based on the CD Bonn potential. Around the cross section minimum, larger contributions of the 3N and 4N forces are partially canceled by the 2N dispersive effect, yielding small net effects of the Δ isobar. The results obtained for the $d\sigma/d\Omega$ are similar to those at 65 MeV, as shown in Fig. 6(a) of Ref. [15]. For the spin correlation coefficient $C_{y,y}$, the effects of the Δ isobar are presented in Fig. 5(b), and are evaluated as

$$\Delta C_{y,y} \equiv C_{y,y}^{\text{CDBonn}+\Delta} - C_{y,y}^{\text{CDBonn}}, \tag{5}$$

where the first (second) term in the right-hand side is the result calculated with the CD Bonn + Δ (CD Bonn) potential. Large Δ-isobar effects are predicted at $\theta_{\text{c.m.}} = 100^\circ$–$140^\circ$. Their angular dependence is similar to that at 65 MeV, while their magnitude is ≈1.5 times larger (see Fig. 6(b) in Ref. [15]). At 65 MeV, the Δ-isobar effects are mostly from the 2N dispersion, and the contributions of the effective 3N and 4N forces are small. Meanwhile, at 100 MeV, the predicted effects of 3N and 4N forces are more enhanced and their size is comparable to that of the 2N dispersive effects. This feature leads to the larger Δ-isobar effects at 100 MeV.

B. Analysis of proton-^{3}He elastic scattering amplitudes

At the present stage, rigorous 4N calculations at intermediate energies are only available for a limited number of nuclear interaction models due to vast requirement of computation resources. Thus we are unable to discuss the present data by directly comparing them with calculations taking into account various models of NN and 3N interactions. Here, instead, we analyze the p-^{3}He elastic scattering amplitudes obtained from the available 4N calculations that are directly related to

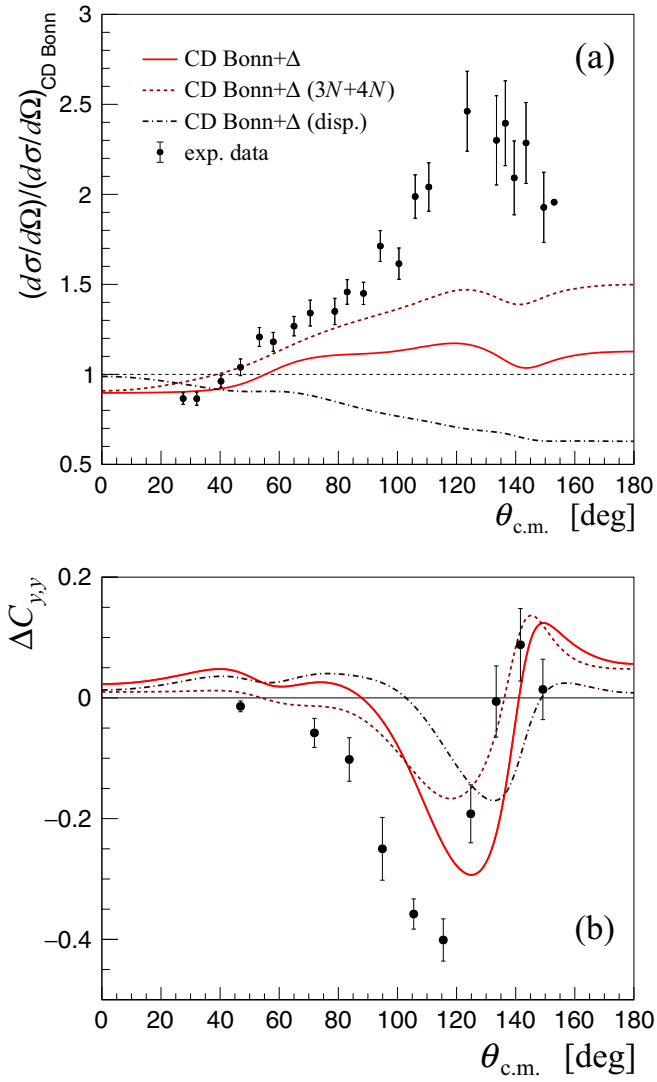

FIG. 5. Effects of the $2N$ dispersion (dot-dashed lines), those of $3N$ and $4N$ forces (dotted lines), and the total Δ-isobar effects (solid lines) in the p-^{3}He elastic scattering at 100 MeV are shown as functions of the c.m. scattering angle for the cross section in the panel (a) and the spin correlation coefficient $C_{y,y}$ in the panel (b). For the cross section, the result of each contribution is shown as a ratio to the prediction based on the CD Bonn potential. For the spin correlation coefficient $C_{y,y}$, the differences from the prediction of the CD Bonn potential, Eq. (5), are presented.

scattering observables. In the spin-space of the p-^{3}He system, namely spin $1/2 \times$ spin $1/2$, there exist six independent complex amplitudes (see, e.g., Ref. [29]). We investigate which parts of the amplitudes are responsible to the discrepancies in the cross section $d\sigma/d\Omega$ and spin correlation coefficient $C_{y,y}$ that are discussed in the previous subsection.

1. Elastic amplitudes and observables

Without loss of generality, the p-^{3}He elastic scattering amplitude can be written in a model interaction form with the spin operator of proton, $\boldsymbol{s}_p$, and that of ^{3}He, $\boldsymbol{s}_h$, as [30,31]

$$\begin{aligned}\boldsymbol{M}(\theta_{\rm c.m.}) &= F_0(\theta_{\rm c.m.}) + (\boldsymbol{s}_p\cdot\boldsymbol{s}_h)F_\sigma(\theta_{\rm c.m.})\\ &+ (\boldsymbol{s}_p\cdot\boldsymbol{n})F_p(\theta_{\rm c.m.}) + (\boldsymbol{s}_h\cdot\boldsymbol{n})F_h(\theta_{\rm c.m.})\\ &+ (\hat{S}_T(\boldsymbol{\ell}) - \hat{S}_T(\boldsymbol{m}))F_{\ell m}(\theta_{\rm c.m.})\\ &+ \hat{S}_T(\boldsymbol{n})F_n(\theta_{\rm c.m.}),\end{aligned} \tag{6}$$

where the vector $\boldsymbol{n}$ is the unit vector normal to both the initial and final momenta in the center-of-mass system, $\boldsymbol{k}_{\rm i}$ and $\boldsymbol{k}_{\rm f}$, respectively. Hereafter, we abbreviate the description of the angular dependence for the amplitude. The vector $\boldsymbol{\ell}$ is the unit vector parallel to $\boldsymbol{k}_{\rm i}+\boldsymbol{k}_{\rm f}$, and $\boldsymbol{m}=\boldsymbol{n}\times\boldsymbol{\ell}$. An operator $\hat{S}_T(\boldsymbol{a})$ is the tensor operator with respect to a unit vector $\boldsymbol{a}$ given as

$$\hat{S}_T(\boldsymbol{a}) = 12(\boldsymbol{s}_p\cdot\boldsymbol{a})(\boldsymbol{s}_h\cdot\boldsymbol{a}) - 4(\boldsymbol{s}_p\cdot\boldsymbol{s}_h). \tag{7}$$

The term $\hat{S}_T(\boldsymbol{\ell})+\hat{S}_T(\boldsymbol{m})$ that possibly arises is included in the $\hat{S}_T(\boldsymbol{n})$ term by using the symmetry relation $\hat{S}_T(\boldsymbol{n})+\hat{S}_T(\boldsymbol{\ell})+\hat{S}_T(\boldsymbol{m})=0$. The functions $F_0, F_\sigma, \ldots$ are the spatial parts of the scattering amplitude, and are classified according to the tensorial property of accompanying operators in the spin space: scalar (rank-0) amplitudes, F_0 and F_σ, describing spin-independent and spin-spin interactions, respectively; vector (rank-1) ones, F_p and F_h, describing the proton spin-orbit (SO) and the ^{3}He SO interactions, respectively; tensor (rank-2) ones, F_n and $F_{\ell m}$.

The $d\sigma/d\Omega$ is expressed by the scattering amplitudes as

$$\begin{aligned}\frac{d\sigma}{d\Omega} &= N\\ &= |F_0|^2 + \frac{3}{16}|F_\sigma|^2 + \frac{1}{4}(|F_p|^2+|F_h|^2)\\ &+ 18|F_{\ell m}|^2 + 6|F_n|^2,\end{aligned} \tag{8}$$

while the spin correlation coefficient $C_{y,y}$ is given as

$$C_{y,y} = \sum_{i=1,4} C_{y,y}^{[i]}, \tag{9}$$

where $C_{y,y}^{[i]}$ $(i=1,\ldots,4)$ are

$$\begin{aligned}C_{y,y}^{(1)} &= \frac{1}{N}{\rm Re}\left\{-\frac{1}{8}|F_\sigma|^2 + \frac{1}{2}(F_0^* F_\sigma)\right\}\\ C_{y,y}^{(2)} &= \frac{4}{N}{\rm Re}\left\{\left(F_0+\frac{1}{4}F_\sigma\right)^* F_n\right\}\\ C_{y,y}^{(3)} &= \frac{1}{2N}{\rm Re}(F_p^* F_h)\\ C_{y,y}^{(4)} &= \frac{1}{N}{\rm Re}\{18|F_{\ell m}|^2 - 2|F_n|^2\}.\end{aligned} \tag{10}$$

Figure 6(a) shows the calculated results of each $C_{y,y}^{(i)}$ $(i=1,\ldots,4)$ contribution to $C_{y,y}$ based on the CD Bonn potential. $C_{y,y}^{(3)}$, which consists of the SO amplitudes, dominantly contributes at the angles $60^\circ \lesssim \theta_{\rm c.m.} \lesssim 140^\circ$. Meanwhile, the contribution of $C_{y,y}^{(2)}$, which contains the scalar and tensor terms, is dominant at backward angles $\theta_{\rm c.m.} \gtrsim 140^\circ$. The effects of the Δ isobar on $C_{y,y}$ and each $C_{y,y}^{(i)}$ $(i=1,\ldots,4)$ are shown in Fig. 6(b). At the angles $60^\circ \lesssim \theta_{\rm c.m.} \lesssim 140^\circ$, the effects of the Δ isobar on $C_{y,y}$ are significant in $C_{y,y}^{(3)}$ and $C_{y,y}^{(1)}$.

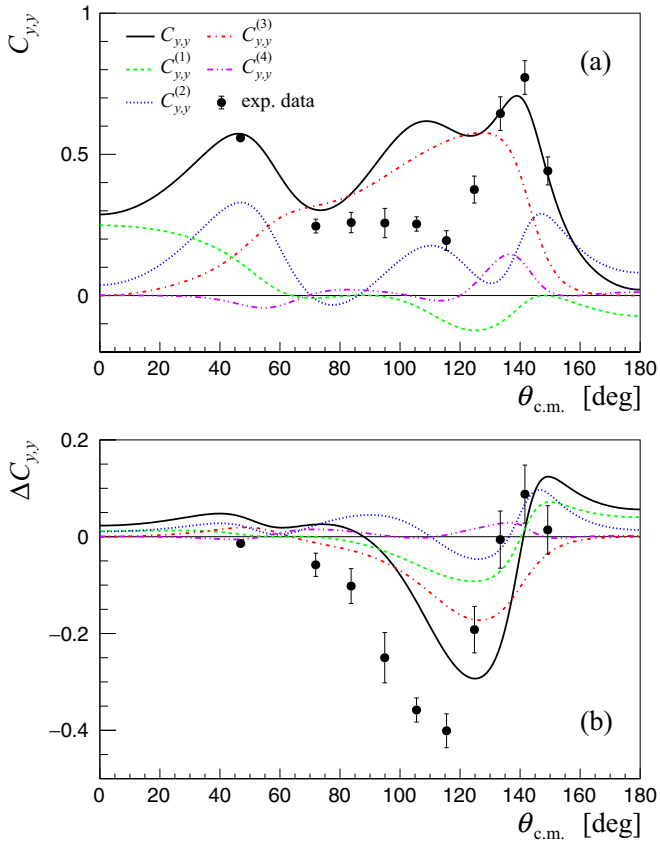

FIG. 6. (a) Angular distributions of $C_{y,y}$ and components $C^{(i)}_{y,y}$ $(i = 1, \ldots, 4)$ for CD Bonn compared with the present experimental data. The thick solid (black) line denotes $C_{y,y}$. Dashed (green), dotted (blue), dot-dashed (red), and dot-dot-dashed (magenta) lines denote $C^{(1)}_{y,y}$, $C^{(2)}_{y,y}$, $C^{(3)}_{y,y}$, and $C^{(4)}_{y,y}$, respectively. (b) Effects of the Δ-isobar on $C_{y,y}$ and components $C^{(i)}_{y,y}$ $(i = 1, \ldots, 4)$ are defined in Eq. (5). The notation of the lines is the same as in panel (a).

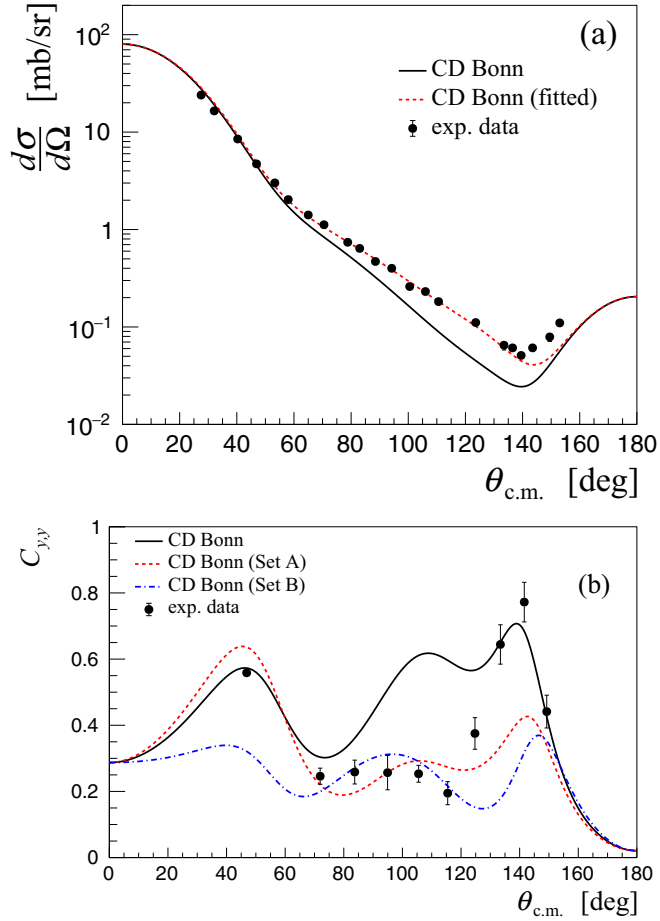

FIG. 7. Calculations with the modified amplitudes of the CD Bonn for (a) the differential cross section and (b) $C_{y,y}$. Solid curves are the results of CD Bonn. In panel (a), the dashed curve is the result for $\lambda_h = 2.4$. In the panel (b), the dashed and dot-dashed curves are the results for set A, $(\lambda_h, \phi_h) = (2.4, 36^\circ)$, and for set B, $(\lambda_h, \phi_h) = (2.4, 251^\circ)$, respectively.

At the backward angles, the Δ isobar effects are mainly from $C^{(1)}_{y,y}$ and $C^{(2)}_{y,y}$.

2. *Fit to the data*

We investigate how the observables $d\sigma/d\Omega$ and $C_{y,y}$ are sensitive to each of the amplitudes $F_0, F_\sigma, \ldots$, for an angular region of $60^\circ < \theta_{\rm c.m.} < 120^\circ$, where the calculations of $C_{y,y}$ with the CD Bonn potential deviate from the data and the Δ-isobar effects are beneficial but not sufficient. For this, we calculate the observables by artificially modifying the amplitude calculated with CD Bonn, one by one, and evaluate the modification by χ^2 values for the experimental data in the above angular region. In this region, we have nine data points for $d\sigma/d\Omega$ and five points for $C_{y,y}$.

First, we calculate the $d\sigma/d\Omega$ replacing an amplitude F_α $(\alpha = 0, \sigma, \ldots)$ by $\lambda_\alpha F_\alpha$, where λ_α is a real value since the $d\sigma/d\Omega$ does not depend on the phase of the amplitudes. Also, the factor λ_α is taken to be independent of the scattering angle for simplicity. It turns out that only the change of F_h with $\lambda_h = 2.4$ gives a reasonable minimum value of $\chi^2/\text{datum} = 1.1$, as shown in Fig. 7(a), while the changes of the amplitudes other than F_h give χ^2/datum larger than 5.

It should be noted that the amplitude F_h is included in $C^{(3)}_{y,y}$, which gives a large contribution to $C_{y,y}$ as well as to the Δ-isobar effects as demonstrated in Figs. 6(a) and 6(b). Considering the form of $C^{(3)}_{y,y}$ given in Eq. (10), we modify the amplitudes as

$$F_p^* F_h \to \lambda_h e^{i\phi_{hp}} F_p^* F_h, \tag{11}$$

where λ_h is fixed to be 2.4 to reproduce the $d\sigma/d\Omega$ reasonably and we omit the parameter λ_p since the absolute value of F_p is unchanged. The parameter ϕ_{hp} denotes a change of the difference of the phase values of F_h and F_p. The $C_{y,y}$ is calculated by varying ϕ_{hp}, and then χ^2 values are obtained for the $C_{y,y}$ data of $60^\circ < \theta_{\rm c.m.} < 120^\circ$. We found two parameter sets providing equally good fits: set A, $(\lambda_h, \phi_{hp}) = (2.4, 36^\circ)$, and set B, $(\lambda_h, \phi_{hp}) = (2.4, 251^\circ)$, as shown in Fig. 7(b). However, in both cases the disagreement with the data is significantly enhanced at $\theta_{\rm c.m.} \gtrsim 130^\circ$.

3. Δ-isobar effects

Referring to the preceding discussion, one may speculate that effects of the Δ isobar on $d\sigma/d\Omega$ and $C_{y,y}$ are represented by the factors λ_h and ϕ_{hp}, calculated with respect to the amplitudes of the CD Bonn potential. Although these values depend on the scattering angle in general, here we pick up a typical angle $\theta_{\rm c.m.} = 120^\circ$. At this scattering angle, the values (λ_h, ϕ_{hp}) for the $\Delta(3N+4N)$, Δ(disp.), and CD Bonn+Δ are $(1.2, 8.2^\circ)$, $(0.8, 3.6^\circ)$, and $(1.0, 13.0^\circ)$, respectively. From these numbers, we see the following characteristics of the Δ effects on $d\sigma/d\Omega$ and $C_{y,y}$, which are consistent with those demonstrated in Figs. 5(a) and 5(b): (i) The values of λ_h indicate enhancement and reduction of the cross section by $\Delta(3N+4N)$ and Δ(disp.), respectively, which leads to small Δ-isobar effects in the $d\sigma/d\Omega$. (ii) The values of ϕ_{hp} for $\Delta(3N+4N)$ and Δ(disp.) indicate that both effects contribute positively to reproduce the $C_{y,y}$ data. (iii) The value of ϕ_{hp} for the total Δ effect being close to but smaller than that of the set A, 36°, indicates that the Δ-isobar effect on $C_{y,y}$ gives the right direction compared to the experimental values, but is not enough to reproduce them.

C. p-^{3}He and proton-deuteron scattering amplitudes

The above discussions show that an improvement of the calculations with the CD Bonn potential for the $d\sigma/d\Omega$ and $C_{y,y}$ in the p-^{3}He elastic scattering at the middle angles can be achieved by changing the vector amplitude in the absolute value and phase. This change is expected to be caused by introducing $3N$ interactions.

Here, for a reference, we demonstrate how $3N$ interactions affect the proton-deuteron (pd) elastic scattering, for which rigorous calculations with varieties of nuclear interaction models are available. Scattering amplitudes and observables for the elastic scattering of proton (spin 1/2) and deuteron (spin 1) are studied in Ref. [32]. For pd elastic scattering, there exist rank-3 amplitudes other than the scalar (rank-0), vector (rank-1), and tensor (rank-2) amplitudes. However they are expected to be negligibly small, and so are omitted in the discussion. Thus, similarly to the p-^{3}He scattering shown in Eq. (8), the $d\sigma/d\Omega$ for the pd elastic scattering consists of contributions from the scalar, vector, and tensor amplitudes, which will be denoted as $N^{[0]}$, $N^{[1]}$, and $N^{[2]}$, respectively. Expressions of $N^{[0]}$, $N^{[1]}$, and $N^{[2]}$ for the p-^{3}He scattering can be read from Eq. (8), e.g. $N^{[0]} = |F_0|^2 + (3/16)|F_\sigma|^2$.

In Figs. 8(a) and 8(b), we show the contributions of each component in $d\sigma/d\Omega$ for the p-^{3}He scattering at 100 MeV and the d-p scattering at 135 MeV/nucleon, respectively. For p-^{3}He scattering, the calculations with CD Bonn and CD Bonn + Δ are shown in comparison with the data of Ref. [16]. For d-p scattering, the calculation including an irreducible $3N$ potential contribution to CD Bonn + Δ, that reproduces the experimental binding energy of ^{3}H, the model U2 [33], is also presented in comparison with the experimental data of Ref. [34].

In both scattering systems, $d\sigma/d\Omega$ at forward and backward angles are dominated by the scalar components $N^{[0]}$. At middle angles, $60^\circ \lesssim \theta_{\rm c.m.} \lesssim 130^\circ$, the scalar components are small. For p-^{3}He scattering at middle angles, a large contribution comes from the vector components $N^{[1]}$. This leads to an expectation that $d\sigma/d\Omega$ and $C_{y,y}$ are sensitive to the magnitude and the phase of the vector amplitude F_h. Meanwhile, for d-p scattering at middle angles, the vector $N^{[1]}$ and tensor $N^{[2]}$ components equally contribute to the $d\sigma/d\Omega$, which gives some complexity to distinguishing contributions from these components.

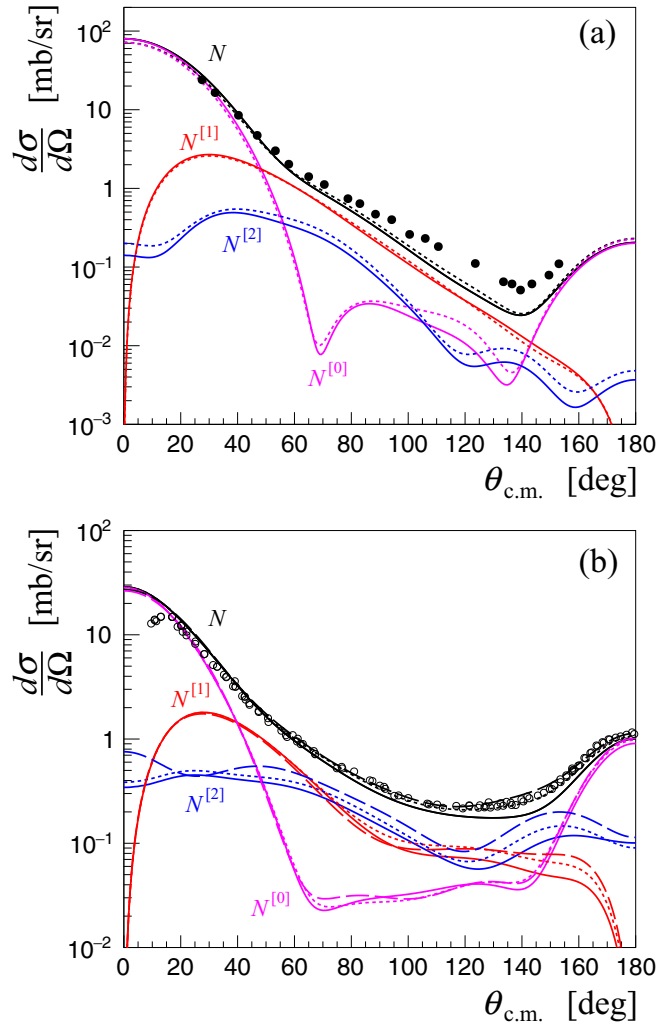

FIG. 8. (a) Differential cross section for p-^{3}He scattering at $E_p =$ 100 MeV. Solid curves are results with CD Bonn, while dashed curves are results with CD Bonn+Δ. Experimental data are taken from Ref. [16]. (b) Differential cross section for d-p elastic scattering at 135 MeV/nucleon. Solid curves are results with CD Bonn, dashed curves are results with CD Bonn+Δ, and long-dashed curves are results with CD Bonn+Δ+U2. Experimental data are taken from Ref. [34].

As demonstrated in Fig. 8(b), for the d-p scattering, the Δ-isobar effects provide sizable contributions and improve the agreement with the experimental data. Effects of the irreducible $3N$ potential are also significant, showing strong evidence for the need to include the $3N$Fs. Notably, these effects are mainly from the vector and tensor amplitudes through the components $N^{[1]}$ and $N^{[2]}$, respectively. This is in contrast to the p-^{3}He scattering, where the effects of the

Δ isobar are small for the dominant component $N^{[1]}$. It is interesting to see how the irreducible $3N$ potential, which gives a sizable effect in the vector amplitude in the d-p scattering, contributes to the p-^{3}He scattering.

IV. SUMMARY AND CONCLUSION

We present the measured spin correlation coefficient $C_{y,y}$ for p-^{3}He elastic scattering at 100 MeV in the angular regime $\theta_{\text{c.m.}} = 46.9°$–$149.2°$. The statistical errors vary from 0.01 to 0.06 depending on the measured angles, and the systematic uncertainties do not exceed the statistical ones.

The new results of the $C_{y,y}$ as well as the previous $d\sigma/d\Omega$ data in Ref. [16] are compared with rigorous $4N$-scattering calculations based on the realistic NN potentials CD Bonn and INOY04. Large differences between the data and the NN force calculations are seen for both observables, especially at the middle angles where the $d\sigma/d\Omega$ takes a minimum. The Δ-isobar effects are estimated by the $NN + N\Delta$ coupled-channels approach. For $d\sigma/d\Omega$, small Δ-isobar effects, caused by the partial cancellation between the effective $3N$ and $4N$ forces and the dispersive Δ-isobar effect, do not explain the differences. The observed feature is similar to that at 65 MeV [15]. In the spin correlation coefficient $C_{y,y}$, larger Δ-isobar effects are predicted than those at 65 MeV, which is due to the feature of Δ-isobar effects of the $3N$ and $4N$ forces being more enhanced at 100 MeV. The agreement with the data is improved by these Δ-isobar effects though the difference still remains around $\theta_{\text{c.m.}} = 90°$.

The analysis of p-^{3}He elastic scattering amplitudes was performed based on the $4N$ calculations with the CD Bonn potential, focusing on middle angles where large differences exist between the data and the $2N$ force predictions. At middle angles, the vector amplitude is the major component in the cross section as well as $C_{y,y}$. The cross section reflects the square of the absolute values of the amplitudes, while the $C_{y,y}$ reflects their phases. Large Δ-isobar effects seen in the $C_{y,y}$ are also sensitive to the relative phase of the vector amplitudes. The vector analyzing powers are known to depend on the phases themselves of the vector amplitudes [30]. Analysis of the analyzing powers at several energies [35] is in progress.

The analysis of the scattering amplitudes was also performed for d-p elastic scattering to investigate the $3N$F effect. The cross section in the minimum region is mainly given by the combination of the vector and tensor amplitudes. These amplitudes provide significant effects of the Δ isobar or the irreducible $3N$ potential, leading to a good description of the data. Meanwhile, in the case of the p-^{3}He scattering, the vector amplitudes which provide small Δ-isobar effects are significant in the cross section minimum region. This indicates necessity of additional $3N$Fs enhancing the vector amplitudes. The features also suggest the possibility of exploring the isospin-3/2 $3N$Fs in p-^{3}He scattering, which are not accessible in d-p scattering.

From these obtained results, we conclude that the spin correlation coefficient $C_{y,y}$ for p-^{3}He elastic scattering at intermediate energies expands the knowledge of nuclear interactions with the Δ isobar or those including $3N$Fs that are masked in N-d elastic scattering. The investigation of the $3N$Fs up to the fifth order based on the χEFT approach, in which rich structure of $3N$Fs is predicted, is in progress [14]. It should be interesting to see how such $3N$Fs affect the p-^{3}He elastic scattering and to explain the data of this scattering system.

ACKNOWLEDGMENTS

We acknowledge the outstanding work of the accelerator groups RCNP for delivering an excellent polarized proton beam. S.N. acknowledges support by GP-PU at Tohoku University. The work of A.D. was supported by Lietuvos Mokslo Taryba (Research Council of Lithuania) under Contract No. S-MIP-22-72. Parts of computations were performed on the supercomputer "VU HPC" of Vilnius University, Faculty of Physics. This work was supported financially in part by JSPS KAKENHI Grants No. JP25105502, No. JP16H02171, No. JP18H05404, and No. JP20H05636.

[1] R. B. Wiringa, V. G. J. Stoks, and R. Schiavilla, Phys. Rev. C **51**, 38 (1995).
[2] R. Machleidt, Phys. Rev. C **63**, 024001 (2001).
[3] V. G. J. Stoks, R. A. M. Klomp, M. C. M. Rentmeester, and J. J. de Swart, Phys. Rev. C **48**, 792 (1993).
[4] P. Reinert, H. Krebs, and E. Epelbaum, Eur. Phys. J. A **54**, 86 (2018).
[5] W. Glöckle, H. Witała, D. Hüber, H. Kamada, and J. Golak, Phys. Rep. **274**, 107 (1996).
[6] J. Carlson, S. Gandolfi, F. Pederiva, S. C. Pieper, R. Schiavilla, K. E. Schmidt, and R. B. Wiringa, Rev. Mod. Phys. **87**, 1067 (2015).
[7] H. Witała, W. Glöckle, D. Hüber, J. Golak, and H. Kamada, Phys. Rev. Lett. **81**, 1183 (1998).
[8] H. Sakai, K. Sekiguchi, H. Witała, W. Glöckle, M. Hatano, H. Kamada, H. Kato, Y. Maeda, A. Nogga, T. Ohnishi *et al.*, Phys. Rev. Lett. **84**, 5288 (2000).
[9] H. Witała, W. Glöckle, J. Golak, A. Nogga, H. Kamada, R. Skibiński, and J. Kuroś-Żołnierczuk, Phys. Rev. C **63**, 024007 (2001).
[10] S. Nemoto, K. Chmielewski, S. Oryu, and P. U. Sauer, Phys. Rev. C **58**, 2599 (1998).
[11] A. Deltuva, R. Machleidt, and P. U. Sauer, Phys. Rev. C **68**, 024005 (2003).
[12] K. Sekiguchi, H. Sakai, H. Witała, W. Glöckle, J. Golak, M. Hatano, H. Kamada, H. Kato, Y. Maeda, J. Nishikawa *et al.*, Phys. Rev. C **65**, 034003 (2002).
[13] E. Epelbaum, J. Golak, K. Hebeler, T. Hüther, H. Kamada, H. Krebs, P. Maris, Ulf-G. Meißner, A. Nogga, R. Roth, R. Skibinski, K. Topolnicki, J. P. Vary, K. Vobig, and H. Witala (LENPIC Collaboration), Phys. Rev. C **99**, 024313 (2019).
[14] E. Epelbaum, J. Golak, K. Hebeler, H. Kamada, H. Krebs, U.-G. Meißner, A. Nogga, P. Reinert, R. Skibiński, K. Topolnicki *et al.*, Eur. Phys. J. A **56**, 92 (2020).

[15] A. Watanabe, S. Nakai, Y. Wada, K. Sekiguchi, A. Deltuva, T. Akieda, D. Etoh, M. Inoue, Y. Inoue, K. Kawahara *et al.*, Phys. Rev. C **103**, 044001 (2021).
[16] N. P. Goldstein, A. Held, and D. G. Stairs, Can. J. Phys. **48**, 2629 (1970).
[17] A. Watanabe, Ph.D. thesis, Tohoku University, 2020 (unpublished).
[18] K. Hatanaka, K. Takahisa, H. Tamura, M. Sato, and I. Miura, Nucl. Instrum. Methods Phys. Res., Sect. A **384**, 575 (1997).
[19] M. Ieiri, H. Sakaguchi, M. Nakamura, H. Sakamoto, H. Ogawa, M. Yosol, T. Ichihara, N. Isshiki, Y. Takeuchi, H. Togawa *et al.*, Nucl. Instrum. Methods Phys. Res., Sect. A **257**, 253 (1987).
[20] M. A. Bouchiat, T. R. Carver, and C. M. Varnum, Phys. Rev. Lett. **5**, 373 (1960).
[21] E. Babcock, I. Nelson, S. Kadlecek, B. Driehuys, L. W. Anderson, F. W. Hersman, and T. G. Walker, Phys. Rev. Lett. **91**, 123003 (2003).
[22] M. V. Romalis and G. D. Cates, Phys. Rev. A **58**, 3004 (1998).
[23] Y. Otake, in *Applications of Laser-Driven Particle Acceleration*, edited by P. Bolton, K. Parodi, and J. Schreiber (CRC, Boca Raton, 2018), Chap. 19, p. 291.
[24] S. Nakai, Ph.D. thesis, Tohoku University, 2021 (unpublished).
[25] A. Watanabe, K. Sekiguchi, T. Ino, M. Inoue, S. Nakai, Y. Otake, A. Taketani, and Y. Wakabayashi, Nucl. Instrum. Methods Phys. Res., Sect. A **1043**, 167486 (2022).
[26] A. Deltuva and A. C. Fonseca, Phys. Rev. C **87**, 054002 (2013).
[27] A. C. Fonseca and A. Deltuva, Few-Body Syst. **58**, 46 (2017).
[28] P. Doleschall, Phys. Rev. C **69**, 054001 (2004).
[29] R. H. Landau and M. Sagen, Phys. Rev. C **33**, 447 (1986).
[30] S. Ishikawa, M. Tanifuji, Y. Iseri, and Y. Yamamoto, Phys. Rev. C **69**, 034001 (2004).
[31] S. Ishikawa, M. Tanifuji, Y. Iseri, and Y. Yamamoto, Phys. Rev. C **72**, 027601 (2005).
[32] S. Ishikawa, M. Tanifuji, and Y. Iseri, Phys. Rev. C **66**, 044005 (2002).
[33] A. Deltuva and P. U. Sauer, Phys. Rev. C **91**, 034002 (2015).
[34] K. Sekiguchi, H. Sakai, H. Witała, W. Glöckle, J. Golak, K. Hatanaka, M. Hatano, K. Itoh, H. Kamada, H. Kuboki *et al.*, Phys. Rev. Lett. **95**, 162301 (2005).
[35] A. Watanabe, S. Nakai, Y. Wada, K. Sekiguchi, T. Akieda, D. Etoh, M. Inoue, Y. Inoue, K. Kawahara, H. Kon *et al.*, Few-Body Syst. **62**, 112 (2021).